Propulsion of microspheres in fluids using rotating magnetic fields

Geir Helgesen[1][2],[a]

[1] Institute for Energy Technology, NO-2027 Kjeller, Norway
[2] Department of Physics, University of Oslo, NO-0316 Oslo, Norway

Abstract. Magnetic microspheres dispersed in fluids can be moved using static field gradients or by applying oscillating or rotating magnetic fields. Such separation methods are useful for many applications within biotechnology and medical technology as a tool to separate or extract cells or molecules. Efficient magnetic separation using field gradients usually requires having a strength of the source of the field of order $B = 1$ T. However, by applying alternating, or rotating, weak magnetic fields with field strength of order $B = 1$ mT, micron sized composite magnetic beads can be controlled and separated. This will happen since the beads are normally much heavier than the surrounding fluid. As the beads due to gravity approach the bottom surface of the sample cell, they may be propelled in a rolling/slipping motion due to a torque from the rotating magnetic field.

1 Introduction

Paramagnetic or ferromagnetic micro- and nanoparticles, which are dispersed in a fluid, can be forced to move when exposed to external magnetic field gradients. This is the basis for magnetophoretic separation techniques [1–3]. Such magnetic microbeads are often made by emulsion polymerization but also a wide range of other preparation techniques exist [4]. Depending on the magnetic moment m_p of the microparticles, the strength H of the external applied field, and the field gradient ∇H, particles are pulled along the magnetic field gradient with a velocity that will be slowed down by the viscous drag on the particle. For sub-micron particles the separation process is very slow due to the competition between magnetic propulsion and Brownian motion. For micrometer sized particles, the speeds will be low due to viscous effects since the Reynolds number Re will be very small ($Re \ll 1$). However, since the liquid volumes in many applications within microfluidics and biotechnology are relatively small, the magnetic particles will often be close to walls. The effect of a wall is normally to slow down any motion due to an increased effective fluid viscosity near the wall, but in some cases the presence of a wall can also be utilized in order to enhance the propulsion. By applying rotating magnetic fields, single magnetic microbeads, or clusters of beads, can be forced to rotate and move [5–12]. A review of the current status of how to activate soft matter with magnetic torque has recently been published [13]. Lim
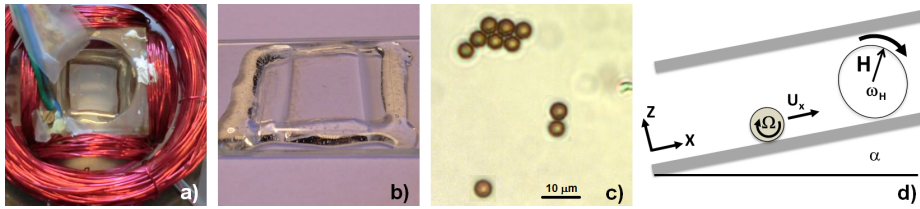
---

[a] e-mail: `geir.helgesen@ife.no`

Fig. 1: (a) Magnet coils with sample seen from above, (b) sealed sample with microspheres, (c) $4.7\,\mu$m magnetic microspheres moving alone or in clusters, and d) schematic drawing of sample cell with a microsphere inside that is rotating at angular velocity Ω and translating at velocity U_x due to a magnetic field $\mathbf{H}$ rotating in the XZ-plane at angular velocity ω_H. The system is tilted an angle α relative to the horizontal plane.

et al. [14] have reviewed how magnetophoretic devices can be used for biomedical applications.

Optical tweezers have been used to trap magnetic microspheres near a surface [15], and the particles were then exposed to rotating magnetic fields. Due to the rotation of the particles, the equilibrium trapping position of the particles was displaced relative to the center of the optical trap. The authors of Ref. [15] then studied how the rolling and slipping of the microsphere depended on the magnetic rotation rate and surface properties. Martinez-Pedrero and Tierno [8] have shown that carpets of magnetically driven rotating beads can be used to carry cargo such as cells. Recently it was proposed that the motion of rotating magnetic beads on inclined planes can be used as a technique for size separation of the beads [16]. The purpose of the current work is to demonstrate that surface friction is the origin of the propulsion force for rotating beads and to show how the propulsion speed depends on particle size, field frequency, and field strength.

2 The experimental setup

The setup consists of an optical microscope, a custom made set of three orthogonal pairs of current carrying coils, and a computer controlled power supply for the magnet coils. The microparticle motion was recorded as videos on a PC using a USB video camera. The amplitudes and phases of the coil currents are checked using a digital oscilloscope. Particle tracks could be extracted directly from AVI-files using the Video_spot_tracker software (www.cismm.web.unc.edu/software/). Figure 1 shows the coil system, the sample cell, and the microspheres inside.

The dry, magnetic microspheres were dispersed in de-ionized water containing 0.1% SDS (Sodium Dodecyl Sulfate) surfactant. The microparticle solution was placed in a sample cell consisting of a microscope glass slide and a cover slide. One layer of double sided tape was used to control the separation between the slides. The cell of size about $15 \times 15\,\text{mm}^2 \times 85\,\mu$m was sealed using epoxy glue [Fig. 1b)]. For the largest particle size (30 μm diameter) double height ($\approx 170\,\mu$m) of the cell was used in some experiments but no clear difference in behaviour relative to using the standard cell was observed. Typically, a current amplitude of $I=1$ A was used to create a field amplitude of about $H=800$ A/m.

The beads used in the current experiments were polystyrene microspheres containing about 24% of iron (magnetite Fe_3O_4/maghemite Fe_2O_3) with a density of $\rho_s \approx 1.6$ g/cm^3. They were provided by the Ugelstad laboratory at NTNU/SINTEF (Trondheim, Norway). Beads of several diameters were explored ($d = 30\,\mu$m, $4.7\,\mu$m,

$3.5\,\mu$m, and $1.5\,\mu$m). Similar particles have been available under various trade names, and their magnetic properties have been characterized by Fonnum et al. [17], who found paramagnetic mass susceptibilities in the range $\chi = 55 - 100 \times 10^{-5}\text{m}^3/\text{kg}$.

In order to avoid many-particle magnetic and hydrodynamic interactions, very dilute mixtures were used inside the sample cells. For each particle size, several samples were studied, and for each sample the motion of two to five particles were recorded. In order to avoid that particles are leaving the field of view of the microscope (about $200\,\mu$m in diameter), the direction of rotation of the magnetic field was changed after time intervals $\Delta t = 10 - 30\,$s.

The microscope system used in the current experiments was placed on a tilt table. This was done in order to be able to compare the motion induced by the rotating magnetic field to the motion induced by gravity in cases when the plane of the sample cell was inclined relative to the horizontal. The velocity due to magnetic propulsion can then be compared to the effective sedimentation velocity due to gravity alone at the same tilt angle. The component of the gravitational force parallel to the surface of the sample cell can be used to "calibrate" the hydrodynamic and frictional forces. The setup for a rotating magnetic bead inside a cell that is tilted an angle α, is shown schematically in Fig. 1d).

3 Theoretical description

3.1 Rotational motion of permanent magnetic moments

For a magnetic microparticle, the magnetic moment generally consists of two parts, the permanent, or remanent, magnetic moment m_p, which will exist in the absence of any external field, and the induced moment $m_H = \chi H V$ due to the magnetic field. Here, $\chi\left(\omega_H\right) = \chi'\left(\omega_H\right) + i \cdot \chi''\left(\omega_H\right)$ is the frequency dependent, complex magnetic susceptibility, H is the field strength, and V is the volume of the particle. The direction of the permanent magnetic moment will be fixed within a microparticle and can be used to define an axis of orientation for a spherical bead. In the case of a magnetic field rotating in a plane, which may be defined as the XZ-plane of the experimental setup, the direction of the permanent moment m_p will form an angle φ_b relative to a predefined X-axis. Janssen et al. [5] have shown that the average angular rotation frequency of a bead, $\langle \Omega_b \rangle$, depends linearly on the magnetic field rotation frequency $f_H = \omega_H/2\pi$. If the magnetic field rotates at an angular frequency ω_H, the magnetic torque τ_m that is acting on the particle will depend on the angle $\theta = \omega_H t - \varphi_b$ between the direction of the field, $\varphi_H = \omega_H t$, and the direction of the permanent magnetic moment, φ_b. The value of this torque is $\tau_m = m_p \mu_0 H \sin(\omega_H t - \varphi_b)$. For stable rotation of a spherical bead, this torque is balanced by a viscous torque τ_v due to the viscosity of the liquid. For rotating beads, a rotational Reynolds number may be defined as $Re = \frac{a^2 \Omega_b}{\nu}$, where $a = \frac{d}{2}$ is the particle radius, $\Omega_b = \frac{\mathrm{d}\varphi_b}{\mathrm{d}t}$ is the angular velocity of rotation, and ν is the kinematic viscosity of the fluid. The Reynolds number for micrometer sized beads is typically in the range $Re \approx 10^{-5} - 10^{-4}$, and thus, all motions are strongly damped. The viscous torque τ_v acting on a rotating bead is given by $\tau_v = -8\pi a^3 \eta \Omega_b$ with $\eta = \nu \cdot \rho$ being the dynamic viscosity for a fluid of density ρ. From this, the rotation of a permanently magnetized bead in a rotating magnetic field is governed by

$$m_p \mu_0 H \sin(\omega_H t - \varphi_b) = 8\pi a^3 \eta \frac{\mathrm{d}\varphi_b}{\mathrm{d}t}. \tag{1}$$

This equation is similar to the Adler equation for oscillators in electrical engineering [18], and it also corresponds to the equation of motion previously found for
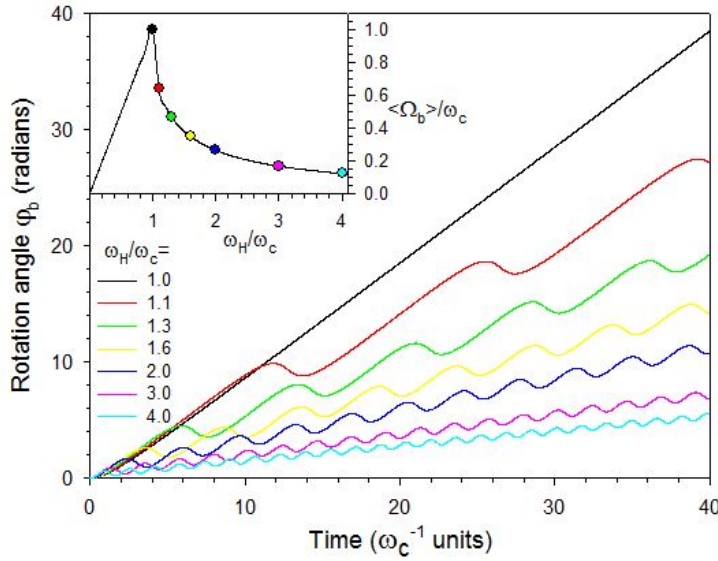
Fig. 2: The angular direction φ_b of a fixed axis within a remanent magnetic microsphere as a function of time for a range of angular frequencies ω_H of a rotating magnetic field. The inset shows the average velocity of bead rotation $\langle \Omega_b \rangle$ as function of ω_H for the curves in the main part (coloured circles) superimposed on the theoretical curve given by Eq. 2 (solid line).

pairs of magnetic holes in ferrofluids [19]. Janssen et al. [5] showed that the magnetic moment m_p was locked to one direction of a fixed axis within magnetic microspheres, as assumed above. For small field angular rotation frequencies ω_H, the direction of orientation of the bead with its fixed moment will lag behind the field by an angle $\theta < \frac{\pi}{2}$. However, at a certain angular frequency $\omega_H = \omega_c$, this phase lag reaches $\theta = \frac{\pi}{2}$. For ω_H slightly larger than ω_c, the phase lag slowly increases beyond $\frac{\pi}{2}$, and the value of the torque decreases until $\theta = \pi$. Then, the torque changes sign. The bead will then during some short time interval rotate in the opposite direction to that of the field. From Eq. 1, the critical frequency for transition from synchronous, stable rotation to asynchronous rotation is $\omega_c = \frac{m_p \mu_0 H}{8\pi a^3 \eta}$. Some rotational motions found as solutions to Eq. 1 are shown in Fig. 2.

For field angular velocity $\omega_H \leq \omega_c$, the lag angle θ increases with ω_H as $\theta = \arcsin\left(\frac{\omega_H}{\omega_c}\right)$, and the bead rotation rate is $\Omega_b = \omega_H$. Above ω_c, the average rotation rate decreases as [20]

$$\langle \Omega_b \rangle = \omega_H - \sqrt{\omega_H^2 - \omega_c^2}. \tag{2}$$

The inset of Fig. 2 shows the linear increase in rotation rate $\langle \Omega_b \rangle$ below $\frac{\omega_H}{\omega_c} = 1$ and the decrease above that value. Thus, at high frequencies the average rate of rotation vanishes.

3.2 Rotational motion of induced moments in superparamagnetic beads

For paramagnetic beads with $m_p = 0$, i.e., superparamagnetic particles, the magnetic moment m_H is induced by the field, and the magnetic torque acting on the

particle in a rotating field is $\tau_H = \chi''(\omega_H)\mu_0 H^2 V$, with $\chi''(\omega_H)$ being the frequency dependent imaginary component (out-of-phase component) of the complex magnetic susceptibility. For monodisperse nanoparticles it can be shown that [5]

$$\chi''(\omega_H) = \chi_0 \frac{\omega_H t_m}{1 + \omega_H^2 t_m^2} \tag{3}$$

with χ_0 the static field susceptibility and t_m the magnetic relaxation time. The time t_m will depend on magnetic domain size and crystalline anisotropy, and is typically in the range $10^{-5}\text{s} < t_m < 10^{-4}\text{s}$ for particles of size $d \approx 20$ nm [22]. In this case, there will be a resonance peak near $\omega_H = \frac{1}{\tau_m}$ and a gradual decrease of χ'' above that. Since composite magnetic microparticles may consist of very many nano-domains with their own relaxation times t_m, one can expect that the imaginary part of the bulk susceptibility will show a much broader response peak than that for a single domain given by Eq. 3. Often, it is assumed that the nano-domain sizes within magnetic beads have a log-normal distribution.

In the general case of a magnetic microspheres, there will be contributions to the torque both from the permanent magnetic moment m_p and from the induced moment m_H, and the balance of torques will be $\tau_m + \tau_H + \tau_v = 0$, as discussed by Janssen et al. [5]. These authors observed a broad peak in bead rotation rate $\langle \Omega_b \rangle$ in the frequency range $f_H = 10^5 - 10^7$ Hz, but also a narrow resonance peak at $f_H \approx$ few Hz was seen.

3.3 Translation of rotating microspheres near surfaces

In many practical cases magnetic beads will be close to a solid surface, like a wall or the bottom of a closed sample cell. Then, the effective hydrodynamic viscosity η_{eff} will deviate from the bulk viscosity η_0 due to the increased drag because the solid surface is within the hydrodynamic disturbance field of the moving or rotating particle. When a spherical bead of radius a is translated in a direction parallel to a planar surface with a minimum separation δ between this surface and the surface of the bead, the increase in translational drag, or alternatively, increase in effective viscosity, is given by [21]

$$\frac{\eta_{eff}^{trans}}{\eta_0} = f_{trans} \approx \frac{8}{15} \ln\left(\frac{a}{\delta}\right) + 0.9588. \tag{4}$$

In a similar way, for a microsphere rotating with an angular velocity vector Ω_b that is parallel to the surface, the increase in rotational drag, or increase in effective rotational viscosity, is [23]

$$\frac{\eta_{eff}^{rot}}{\eta_0} = f_{rot} \approx \frac{2}{15} \ln\left(\frac{a}{\delta}\right) - 0.2526. \tag{5}$$

For beads close to a wall, these effects may be very important, e.g., the factors f_{trans} and f_{rot} are about 2.6 and 0.15, respectively, at $\frac{\delta}{a} = 0.05$.

Now, consider the situation with a magnetic microsphere that is in contact with a planar surface due to the density mismatch $\Delta\rho = \rho_s - \rho_l$ between the solid bead and the liquid. In a general case, the bottom surface of the sample cell can be tilted by an angle α relative to the horizontal plane. The X-axis of the coordinate system is along the direction of forced motion of the bead. For a tilted surface, the positive X-axis direction can be chosen to be pointing "uphill" along the surface as shown in Fig. 1d). The Y-axis is then along the perpendicular direction parallel to the surface. The bead is acted on by an external magnetic field rotating in the XZ-plane with angular frequency ω_H. The induced magnetic torque will force the bead to rotate.

The forces acting on the bead are gravity, $W_g = \frac{4}{3}\pi a^3 \Delta\rho g$, a surface normal force N_c in the contact point between bead and surface, a lift force L_h due to a hydrodynamic lift at finite Reynolds number, a friction force $F_f = \mu_k N_c$ acting in the contact point parallel to the surface with μ_k being the kinetic friction coefficient, and a viscous drag force F_h due to the translation and rotation of the bead. This viscous drag is always opposite to the direction of motion.

Now, assume that the bead is rotating about the Y-axis of the coordinate system with an angular velocity Ω_b and is moving at a velocity U_x in the X-direction. The rotation of the microsphere may not follow the rotation of the magnetic field, but the motion can be partly rolling and partly slipping, and this "skipping" can be modeled through a slipping coefficient γ as $U_x = \gamma a \Omega_b$. Then, the total viscous drag force F_h acting on the sphere can be written as [16]

$$F_h = 6\pi\eta_0 a \left(-f_{trans} \cdot U_x + f_{rot} \cdot a\Omega_b\right) = -6\pi\eta_0 a U_x \left(f_{trans} - \frac{1}{\gamma} \cdot f_{rot}\right). \quad (6)$$

When a rigid sphere is moving very close to a planar surface, there will be a small lift force on the sphere pushing it away from the surface in the surface-normal Z-direction. This will happen when the planar surface is within the disturbance flow-field of the sphere [24]. However, for the bead rotation frequencies Ω_b that can be obtained using paramagnetic beads, typically $\Omega_b \ll 100\,\mathrm{s}^{-1}$, this effect is negligible [25].

It can then be shown that the velocity of the microsphere is given by [25]

$$U_x = U_s \cdot \frac{\varepsilon\mu_k \cos\alpha - \sin\alpha}{f_{trans} - \frac{1}{\gamma} \cdot f_{rot}}, \quad (7)$$

where U_s is the so-called sedimentation velocity, and with $\varepsilon = +1$ for uphill motion and $\varepsilon = -1$ for downhill motion in the case of a tilted surface. The sedimentation velocity, $U_s = \frac{2}{9}\Delta\rho g a^2/\eta_0$, is the velocity of a sphere that is falling freely inside the liquid, $g = 9.81\,\mathrm{m/s}^2$ the acceleration of gravity, and η_0 the dynamic, bulk viscosity of the liquid. For the present experiments with water at a temperature of about $T = 30°\mathrm{C}$, $\Delta\rho = \rho_s - \rho_l = 600\,\mathrm{kg/m}^3$ and $\eta_0 = 0.80\,\mathrm{mPa\cdot s}$, one finds $U_s = 9.0\,\mu\mathrm{m/s}$. For spheres that are propelled on a horizontal surface ($\alpha = 0$), the velocity will be

$$U_x = U_s \cdot \frac{\mu_k}{f_{trans} - \frac{1}{\gamma} \cdot f_{rot}}. \quad (8)$$

Thus, the speed depends on the surface friction coefficient μ_k, the slipping coefficient γ, and the effective sphere to surface separation δ (through $f_{trans}(\delta)$ and $f_{rot}(\delta)$).

4 Results and discussion

Figure 3 shows two examples of digitally calculated traces for the motion of microspheres being propelled inside a horizontally oriented glass sample cell of thickness about 85 μm. The bead was driven by a rotating field of frequency $f_H = 100\,\mathrm{Hz}$ and amplitude $H = 1.1\,\mathrm{kA/m}$. The plane of the rotating field was perpendicular to X-Y field of view. The patterns of motion were programmed into the digital-to-analog converter that was driving the magnet coils, and the same motion could be repeated several times. The bead was every time passing through almost exactly the same locations in the sample cell. This demonstrates the accuracy that can be obtained for this type of magnetic particle control. For the smaller bead sizes ($d < 5\,\mu$m), a Brownian component of the motion could be seen as a small wiggling movement.
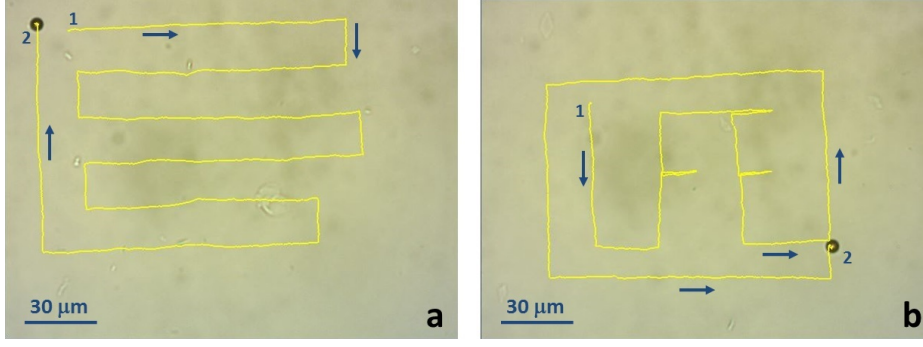
Fig. 3: The digitally recorded traces of a $d = 4.7\,\mu$m beads being propelled by a rotating magnetic field at the interface between water and a horizontal glass surface. The motion started at position 1 and ended at position 2. The field amplitude was $H = 1.1\,$kA/m in the XZ- or YZ-planes and the rotation frequency $f_H =100$ Hz. Field-of-view: $X \times Y = 185 \times 140\,(\mu$m$)^2$.
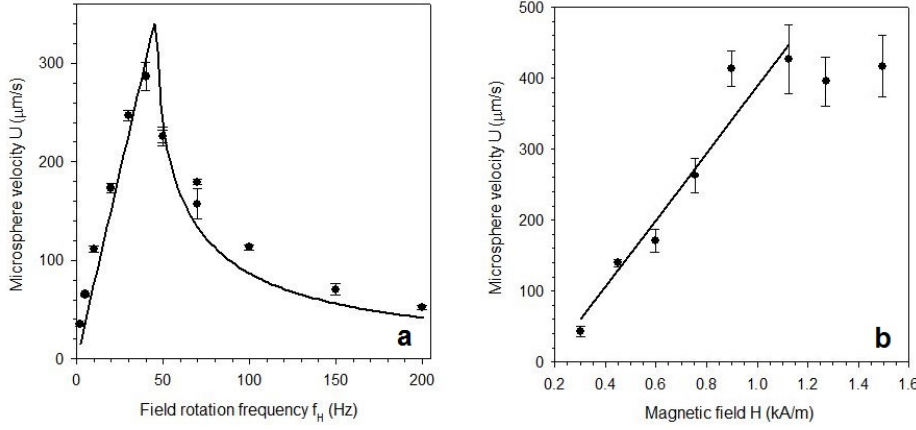

Fig. 4: (a) Propulsion velocity U vs. magnetic field rotation frequency f_H for microspheres of diameter $d = 30\,\mu$m. The field amplitude was $H = 1.1$ kA/m. The solid line is a fit to a model for U similar to the oscillating dipole model of Eq. 2 with $f_c = 46$ Hz. (b) Velocity U as function of field amplitude H at $f_H = 40$ Hz for this microsphere size. The solid line is a guide to the eye.

4.1 Propulsion of remanent magnetic beads

The propulsion velocity for $d = 30\,\mu$m beads as function of magnetic field strength and rotation frequency is shown in Figure 4. The velocity shows a sharp peak near $f_H \approx 45$ Hz and decreases gradually above that frequency as the bead entered the asynchronous mode of rotation. These microspheres have a remanent magnetization, and then their average angular rotation frequency $\langle \Omega_b \rangle$ can be described by Eq. 2. In a rolling-slipping model the velocity U of the bead will be directly proportional to its average angular velocity, and a similar functional form as Eq. 2 can be used for the velocity. The best fit to this model is shown as a solid curve in Fig. 4a) with a value $f_c = \frac{\omega_c}{2\pi} = 46$ Hz for the critical field rotation frequency. The existence of a remanent magnetic moment for the 30 μm particles can be seen in Fig. 4 b), which shows the velocity as a function of magnetic field amplitude H. The velocity increases linearly
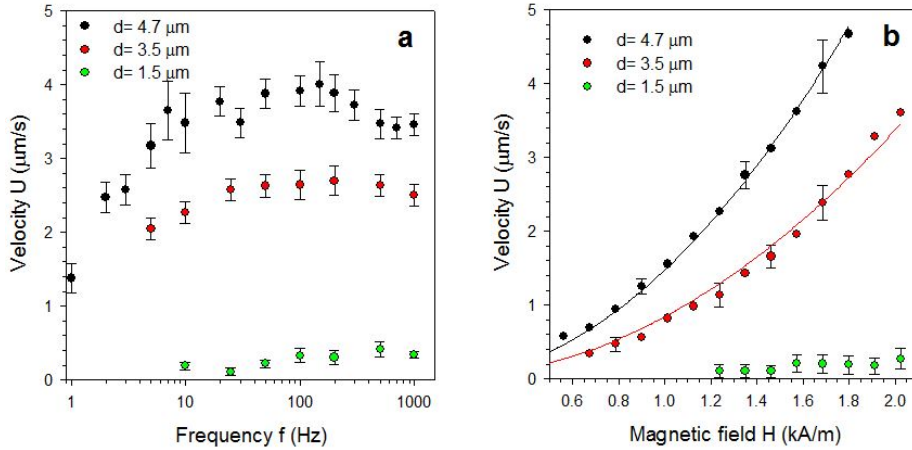
Fig. 5: a) Velocity of microspheres of three different diameters d as function of field rotation frequency f_H. The data for $4.7\,\mu$m and $3.5\,\mu$m beads were measured at field $H = 1.1\,\mathrm{kA/m}$, and for $d = 1.5\,\mu$m the field was $H = 2.2\,\mathrm{kA/m}$. b) Velocity as function of the amplitude H of the magnetic field measured at $f_H = 100\,\mathrm{Hz}$. Solid lines are regression fits to $U \propto H^2$.

with magnetic field as it will do for permanent magnetic dipoles since $U = \gamma a \Omega_b \propto H$ according to Eq. 1. For a superparamagnetic bead, the velocity and magnetic torque would go as $U \propto \tau_H \propto H^2$ as has been reported for smaller sized microspheres [5, 25]. For fields above about $H \approx 1\,\mathrm{kA/m}$, it looks like the magnetic moment was saturated, and the velocity remained nearly constant. It may be noted that the data in Fig. 4a) could not be approximated by using a susceptibility of the form given by Eq. 3, which gives a much too broad resonance peak even when using only one value of t_m for all magnetic domains.

4.2 Propulsion of superparamagnetic beads

The propulsion velocities for smaller particles, $d = 4.7\,\mu$m, $3.5\,\mu$m, and $1.5\,\mu$m, are shown in Fig. 5. At a frequency of $f_H = 100\,\mathrm{Hz}$, the ratio of the best fit amplitudes $A_{4.7}$ and $A_{3.5}$ for the relation $U = A \cdot H^2$, which are shown as solid lines in Fig. 5b), is $\frac{A_{4.7}}{A_{3.5}} = 1.75$. According to Eq. 8, the ratio of the velocities should be proportional to the ratio of sedimentation velocities since the surface drag correction factors (f_{trans}, f_{rot}) are very weakly dependent on particle size ratio (less than 5% difference in the present case). Since $U_s \propto a^2$, the velocities should scale with a factor $\left(\frac{4.7}{3.5}\right)^2 = 1.8$, in good agreement with the ratio found from measurements. Comparing velocities of $d = 30\,\mu$m and $4.7\,\mu$m particles at similar fields and frequencies (e.g., 100 Hz, 1.1 kA/m in Fig. 4), the velocity ratio is $\frac{U_{30}}{U_{4.7}} = 55$ while the diameter ratio squared is about 41. However, the $d = 30\,\mu$m particles have a remanent magnetization, and thus, a direct scaling of size and speed cannot be expected.

The $d = 1.5\,\mu$m beads did only show a very weak frequency and field amplitude dependence. As seen in Fig. 5, the velocity of these beads was reduced by a factor of more than ten as compared to the $d = 3.5\,\mu$m particles. Bead diameter alone can only account for about half of this velocity reduction. However, in this case particle velocity was averaged over typical measurement times of $t = 100\,\mathrm{s}$. The typical diffusion distance σ_d that a particle can be moved by Brownian motion during this time interval
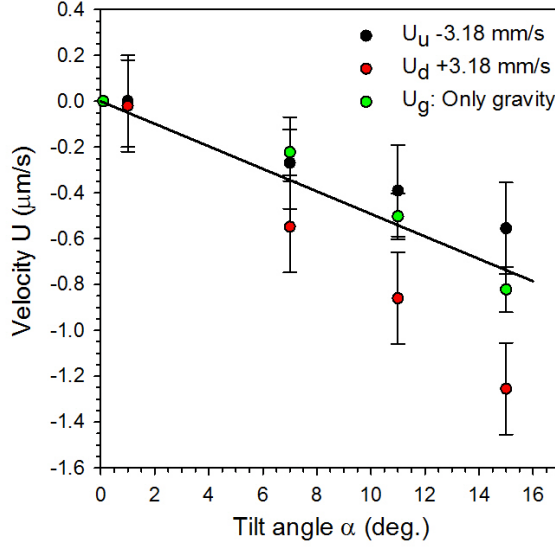
Fig. 6: The velocity of $d = 4.7\,\mu$m beads being propelled uphill (U_u) or downhill (U_d) by a $H = 1.1$ kA/m field rotating at frequency 100 Hz for various values of the sample tilt angle α. The green symbols show the velocity U_g of downhill rolling motion due to gravity alone. The curves for U_u and U_d have been shifted to make a comparison to the effect of gravity easier. The solid line shows a linear regression fit to the data for U_g. The slope B of this line is $B = -0.049\,\frac{\mu\mathrm{m}}{s\cdot\mathrm{deg.}}$.

is $\sigma_d = \sqrt{2Dt}$, where $D = \frac{k_B T}{6\pi\eta_0 a}$ is the diffusion constant, k_B the Boltzmann constant, and $T = 300$ K the sample temperature. Then, $\frac{\sigma_d}{t} \approx 0.1\,\mu$m/s, and a large fraction of the variation in particle velocity can be attributed to diffusion and not to effects of the magnetic propulsion. For even smaller magnetic beads, $d < 1\,\mu$m, the diffusion will be even more dominating, and very strong fields may be needed to overcome the effects of diffusion on the motion of the beads. This trend of reduced propulsion with decreasing particle size may be seen even clearer by calculating the Péclet number, $Pe = \frac{U \cdot a}{D}$, which is 80, 30, and 0.8 for $d = 4.7\,\mu$m, $3.5\,\mu$m, and $1.5\,\mu$m beads, respectively.

For magnetic propulsion using similar type of beads, it has been reported that due to microsphere surface roughness the hydrodynamic effective separation δ between bead surface and glass surface may be about $\delta \approx 20$ nm, the slipping coefficient was $\gamma \approx 0.6$, and the surface friction coefficient $\mu_k \approx 0.5$ [25]. Figure 6 shows how the propulsion velocity depends on the tilt angle α of the sample cell (measured relative to the horizontal plane). For $d = 4.7\,\mu$m beads, using a field frequency of 100 Hz and a field amplitude of $H = 1.1$ kA/m, the average velocity of beads moving on a horizontal surface was $U(\alpha = 0) = 3.18\,\mu$m/s. In order to see more clearly the effect of gravity on the motion, this velocity has been subtracted off the data in Fig. 6, which thus shows how the velocity was reduced due to gravity effects when microspheres were moving "uphill" (U_u) or "downhill" (U_d). The figure also shows the velocity U_g of beads when there was no magnetic field and the beads were slowly rolling downhill due to their higher density. The solid line shows a linear regression fit for the gravity only data, $U_g = B \cdot \alpha = -0.049\,\mu$m/s$\cdot \alpha$(deg.) $= -2.8\,\mu$m/s$\cdot \alpha$(rad.). This velocity is in good agreements with what has been reported before for this type of particles [25]. Now, using Eqs. 4 and 5 with an effective hydrodynamic separation
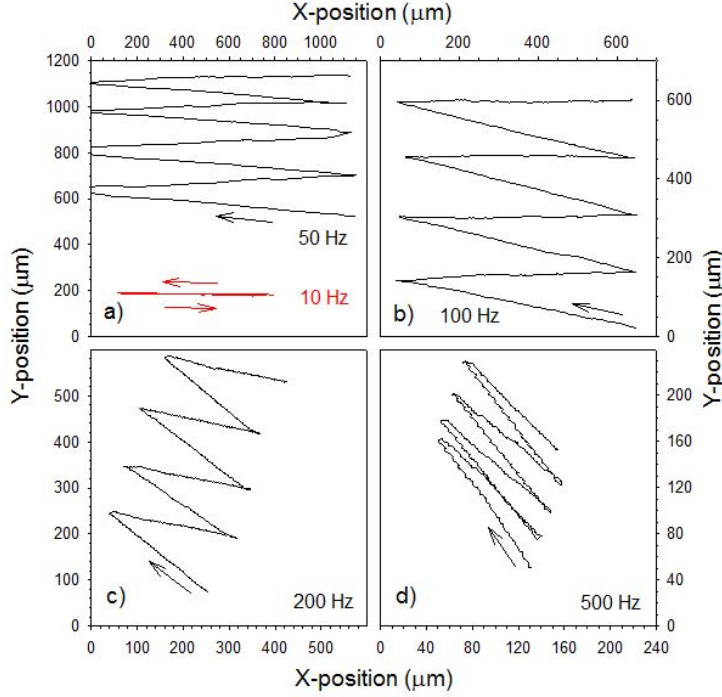
Fig. 7: Recorded traces of $d = 30\,\mu$m beads in a magnetic field of amplitude $H = 1.1$ kA/m rotating in the XZ-plane. The direction of rotation was changes between clockwise and anti-clockwise every 10 s. a) For $f_H = 10$ Hz (red curve) the motion of the beads is parallel to the plane of the rotating field but at a higher frequency $f_H = 50$ Hz (black curve) there is also a component of the motion perpendicular to the field, i.e. along the Y-axis. The deviation of direction of motion away from that of the field increases at higher frequencies, such as b) 100 Hz, c) 200 Hz, and d) 500 Hz. Note the different scales on the axis in the four parts.

$\delta \approx 20$ nm, surface friction coefficient $\mu_k \approx 0.5$ [25], and $U(\alpha = 0) = 3.18\,\mu$m/s, the surface slipping coefficient γ can be calculated from Eq. 8. The slipping coefficient may depend on the bead rotation speed and the driving magnetic torque, and these depend on magnetic field parameters. Here, for the present case one finds $\gamma \approx 0.19$. This corresponds to an angular rotation frequency $\Omega_b = \frac{U}{\gamma a} = 7.1\,\text{s}^{-1}$ or frequency of bead rotation $f_b = 1.1$ Hz. This value of γ can be compared to the value $\gamma \approx 0.6$, which was found for a smaller field amplitude [25]. As seen in Fig. 6, the change in velocity with tilt angle is slightly smaller for uphill motion (black data points), and it is slightly larger for downhill motion (red data points) than what can be found for pure gravity effects (green data points). This can possibly be due to a coupling of the translational, f_{trans}, and rotational, f_{rot}, viscosity correction coefficients for higher speeds, thus invalidating the assumption of additivity of the two drag effects.

4.3 Motion of remanent magnetic beads in asynchronous rotation

The motion of the superparamagnetic microspheres always appeared to be along the line created by the intersection of the surface and the plane of the rotating field. However, for the large particles with a remanent magnetic moment, the behaviour

was different. Figure 7 shows the recorded traces for the motion of $d = 30\,\mu$m spheres inside a horizontal sample cell with the magnetic field rotating in the XZ-plane. Here, the rotation was first counter-clockwise in the XZ-plane, and after a time interval $\Delta t = 10$ s was changed to clockwise rotation for the next 10 s. This procedure was repeated four times. For field rotation frequencies below the critical frequency of stable rotation, $f_H < f_c$, the velocity was parallel to the plane of the rotating field for both clockwise and counter-clockwise direction of rotation. This is exemplified by the trace for $f_H = 10$ Hz shown as the red lines parallel to the X-axis in Fig. 7a). Figure 7a)-d) shows how the direction of propulsion of the microsphere moves out of the XZ-plane of the rotating field for frequencies in the asynchronous mode above the critical value $f_c \approx 46$ Hz. In Fig. 7a), the black curve for $f_H = 50$ Hz shows that the motion was now only partly parallel to the field, and its direction changed by an angle of about 8° every time the direction of rotation changed. This shift in direction for every change of direction of rotation increased to about 14° at $f_H = 100$ Hz [Fig. 7b)]. As the component of motion perpendicular to the plane of the magnetic field rotation (the Y-component) increased, this twist of the direction of particle rotation decreased [Fig. 7c)-d)].

As discussed in Section 3.1, above a critical frequency $\omega_c = 2\pi f_c$ of Eq. 1, the particle rotation was unstable, as was illustrated in Fig. 2. The direction of the dipole moment will then perform a forward-backward loop to catch up with the phase of the rotating field. In real, practical cases the magnetic moment may not be limited to move in the plane of the rotating field, and there may be a small component of the magnetization perpendicular to this plane. The reason for this out of plane component can be the distribution of domains within the bead. Thus, it may be advantageous for the magnetic moment in this mode of motion to move out of the plane of the rotating field and perform a precessing motion, which will bring the motion of the bead into a path that makes an angle to the plane of the rotating field. Every time the direction of field rotation changed between clockwise and counter-clockwise, the torque induced by the component of magnetization perpendicular to the field turned the axis of bead rotation by a small angle. Since the speed of motion is largest near f_c, the total distance that a microsphere moves during a fixed time interval (here $\Delta t = 10$ s) will also be largest near f_c, and therefore, this zigzag pattern of motion will be most easily observed just above f_c. Agayan et al. [15] observed similar effects in rotating fields for both free microspheres on a glass surface, as well as for microspheres that were trapped by optical tweezers at the surface, and found shifts in the direction of motion relative to the plane of the rotating field of up to 10° for field rotation frequency above a critical value $f_c \approx 2.5$ Hz. This was interpreted as a tilt of the direction of the magnetic moment away from the plane of rotation into the third dimension.

Similar shifts in the direction of motion have been observed for the rolling of magnetic, colloidal wheels by Maier et al. [26]. When the plane of the rotating wheel was not perpendicular to the surface below, the wheel performed a zigzag trajectory as the direction of field rotation was changed. Complex patterns of motion for magnetic particles in oscillating field have previously been reported for, e.g., magnetotactic bacteria [27] and for magnetic Janus colloids [28]. In both of these cases, there was an anisotropy in the magnetization distribution relative to that of the mass distribution. In the present case, it may be assumed that the distribution of magnetic material has a spherical symmetry, but with a preferred orientation of the magnetic nano-domains. A theoretical study of anisotropic ferromagnetic particles in rotating fields [29] has shown a complicated phase diagram of the modes of motion, which will depend on both the field rotation frequency and the strength of the magnetic field relative to a nominal field strength calculated from the magnetic domain anisotropy energy. Both rotating and precessing modes of motion were predicted. Thus, in order to be able to control the speed and direction of motion when remanent magnetic beads are

propelled by rotating magnetic fields, one may need to use field frequencies below the threshold frequency f_c for transition from synchronous to asynchronous rotation. This critical frequency depends on field strength as $f_c \propto H$.

4.4 Further comments

The measured velocities for horizontal sample can be compared to those reported by Martinez-Pedrero et al. [8,9], who found speeds of $0.6\,\mu\mathrm{m/s}$ and $\sim 1\,\mu\mathrm{m/s}$ for paramagnetic microspheres of diameter $d = 2.8\,\mu\mathrm{m}$ at field rotation frequencies of 10 Hz and 150 Hz, respectively. These authors also reported about "colloidal micro-worms" consisting of the collective motion of two or more beads propelled by elliptically polarized magnetic fields. The propulsion speed increased from about $1\,\mu\mathrm{m/s}$ up to about $5\,\mu\mathrm{m/s}$ when the number of beads in a chain increased from two up to about 30. Assuming no contact between the microspheres and the surface (neutrally buoyant spheres, $\Delta\rho \approx 0$), these authors were able to model the motion as due to the anisotropic hydrodynamic flow field near the surface. From this a surface-surface separation of about $\delta \sim 180\,\mathrm{nm}$ could be deduced. Using a small rotating component of the magnetic field in the sample plane in addition to the component rotating perpendicular to this plane, it was shown that propelled "colloidal carpets" could be formed [8]. These were planar assemblies of typically 10-100 beads that were controlled by rotating magnetic fields, and could be used to transport cargo such as a single cell loaded on top. In the experiments reported her, similar many-body structures could be observed when elliptically polarized fields were applied. In agreement with what was reported in Ref. [8], the propulsion velocity U increased nearly logarithmically with number N of particles, $U \sim \log(N)$ for these assemblies of beads, going from about $U = 4\,\mu\mathrm{m/s}$ for $N = 4$ up to $\approx 10\,\mu\mathrm{m/s}$ for $N > 30$ (at $f_H = 100\,\mathrm{Hz}$, $H = 1.1\,\mathrm{kA/m}$). However, since the density mismatch $\Delta\rho$ of the microspheres that were used here was large, and the angular rotation velocities were low ($\Omega_y \sim 1 - 10\,\mathrm{s}^{-1}$), the hydrodynamic lift cannot move the beads away from the surface. Therefore, surface frictional force was the main reason for propulsion in these experiments.

Magnetic microbeads are popular for various types of magnetic sorting for cell isolation [1]. This can be done, e.g., by using antibody-antigen capture or by the strong streptavidin-biotin binding to the surface of coated magnetic beads (e.g. the commercially available Dynabeads). Antibody coated beads may be used for differentiation of cardiomyocytes [30] and may also be used in immunosorbent assays to detect e.g. proteins [31]. Superparamagnetic beads on specially designed surfaces, which had a magnetic disk pattern, have been explored for potential use in cell separation for lab-on-a-chip [32]. These authors found a particle dynamics which looks similar to the one found in the present experiments, but the motion was limited to a small region around each magnetic disk of diameter 10-30 μm. Lim et al. [33] have designed a similar system of connected magnetic disks and demonstrated control and separation of both single beads as well as antibody coated beads carrying a cell cargo. In these applications, either static magnetic fields or fields rotating in the plane of the sample cell were used. In the present experimental setup, the magnetic fields are rotating perpendicular to the bottom surface of the cell containing the sample. This opens up possibilities for full control of the direction of particle propulsion. Using microfluidic cells containing several inlets and outlets, microspheres may be injected to the cell, pick up their cargo (live cells or protein molecules) using antibody-antigen reactions, and then be moved to the appropriate outlet where bead and cargo can be collected. Further studies may explore the effect of the bead rotation on the bead-cargo chemical binding. By applying tilted sample cells, or sample cells with a prepared surface ratchet configuration [16], magnetic beads may also be sorted according to their size or their magnetic moment.

5 Conclusion

Experiments demonstrating the propulsion of few-μm sized magnetic spheres at a fluid-glass interface have been presented. The propulsion was due to surface frictional forces acting on the rotating magnetic beads. The direction of the magnetic torque driving the beads can be controlled externally via the electric currents in three orthogonal pairs of magnet coil in the reported setup. This allows for motion in any direction parallel to the interface, and the speed of motion will be from less than $1\,\mu$m/s up to a maximum speed that is limited by the field driving frequency and the field amplitude. In this report, speeds up to ten times the particle diameter per second have been shown for large particles with remanent magnetization, and speeds up to about one bead diameter per second have been observed for smaller, superparamagnetic beads. The positioning and motion of the beads could be programmed from a PC, and the repeatability was mainly limited by Brownian diffusion effects. The proposed setup may have application for sorting magnetic beads, as well as within biomedical cell/molecule separation and sorting.

Acknowledgments

References

1. B.D. Plouffe, S.K. Murthy, L.H. Lewis, Rep. Prog. Phys. **78** 016601 (2015)
2. P. Tierno, Phys. Chem. Chem. Phys. **16**, 23515 (2014)
3. R.S.M. Rikken, R.J.M. Nolte, J.C. Maan, J.C.M. van Hest, D.A. Wilson, P.C.M. Christianen, Soft Matter **10**, 1295 (2014)
4. D. Xiao, T. Lu, R. Zeng, Y. Bi, Microchimica Acta **183**, 2655 (2016)
5. X.J.A. Janssen, A.J. Schellekens, K. van Ommering, L.J. van Ijzendoorn, M.W.J. Prins, Biosensors and Bioelectronics **24**, 1937 (2009)
6. H. Morimoto, T. Ukai, Y. Nagaoka, N. Grobert, T. Maekawa, Phys. Rev. E **78**, 021403 (2008)
7. C.E. Sing, L. Schmid, M.F. Schneider, T. Franke, A. Alexander-Katz, Proc. Natl. Acad. Sci. U.S.A. **107**, 535 (2010)
8. F. Martinez-Pedrero, P. Tierno, Phys. Rev. Appl. **3**, 051003 (2015)
9. F. Martinez-Pedrero, A. Ortiz-Ambriz, I. Pagonabarraga, P. Tierno, Phys. Rev. Lett. **115**, 138301 (2015)
10. T.O. Tasci, P.S. Herson, K.B. Neeves, D.W.M. Marr, Nature Commun. **7**, 10225 (2016)
11. H. Massana-Cid, F. Martinez-Pedrero, E. Navarro-Argemi, I. Pagonabarraga, P. Tierno, New J. Phys. **19**, 103031 (2017)
12. F. Martinez-Pedrero, H. Massana-Cid, P. Tierno, Small **13**, 1603449 (2017)
13. R. M. Erb, J.J. Martin, R. Soheilian, C. Pan, J.R. Barber, Adv. Funct. Mater. **26**, 3859 (2016)
14. B. Lim, P. Vavassori, R. Sooryakumar, C. Kim, J. Phys. D: Appl. Phys. **50**, 033002 (2017)
15. R.R. Agayan, R.G. Smith, R. Kopelman, J. Appl. Phys. **104**, 054915 (2008)
16. M.M. Rashidi, S. Johnson, Z. Yang, J. Magn. Magn. Mater. **398**, 13 (2016)
17. G. Fonnum, C. Johansson, A. Molteberg, S. Mørup, E. Aksnes, J. Magn. Magn. Mater. **293**, 41 (2005)

18. R. Adler, Proc. Inst. Radio Engineers **34**, 351 (1946)
19. G. Helgesen, P. Pieranski, and A.T. Skjeltorp, Phys. Rev. Lett. **64**, 1425 (1990)
20. G. Helgesen, P. Pieranski, and A.T. Skjeltorp, Phys. Rev. A **42**, 7271 (1990)
21. A.J. Goldman, R.G. Cox, H. Brenner, Chem. Eng. Sci. **22**, 637 (1967)
22. F. Ludwig, C. Balceris, C. Jonasson, C. Johansson, IEEE Trans. Magnetics **53**, 6100904 (2017)
23. Q. Liu, A. Prosperetti, J. Fluid Mech. **657**, 1 (2010)
24. P. Cherukat, J.B. Mclaughlin, J. Fluid Mech. **263**, 1 (1994)
25. G. Helgesen, J. Appl. Phys. **123**, 064902 (2018)
26. F.J. Maier, T. Lachner, A. Vilfan, T.O. Tasci, K.B. Neeves, D.W.M. Marrc, T.M. Fischer, Soft Matter **12**, 9314 (2016)
27. K. Erglis, Q Wen, V. Ose, A. Zeltins, A. Sharipo, P. A. Janmey, and A. Cebers, Biophys. Journal **93**, 1402 (2007)
28. J. Yan, M. Bloom, S.C. Bae, E. Luijten, S. Granick, Nature **491**, 578 (2012)
29. J. Cimurs, A. Cebers, Phys. Rev. E **88**, 062315 (2013)
30. V. Schwach, R. Passier, Differentiation **91**, 126 (2016)
31. S. K.Vashist, G. Czilwik, T. van Oordt, F. von Stetten, R. Zengerle, E.M. Schneider, J.H.T. Luong, Anal. Biochem. **456**, 32 (2014)
32. X. Hu, R. Abedini-Nassab, B. Lim, Y. Yang, M. Howdyshell, R. Sooryakumar, B.B. Yellen, and C. Kim, J. Appl. Phys. **118**, 203904 (2015)
33. B. Lim, V. Reddy, X. Hu, K. Kim, M. Jadhav, R. Abedini-Nassab, Y.W. Noh, Y.T. Lim, B.B. Yellen, C. Kim, Nature Communications **5**, 3856 (2014)